

# On the identification of earlywood and latewood radial elastic modulus of *Pinus pinaster* by digital image correlation: A parametric analysis

*J Strain Analysis*

1–9

© IMechE 2018

Reprints and permissions:

sagepub.co.uk/journalsPermissions.nav

DOI: 10.1177/0309324718786351

journals.sagepub.com/home/sj



João Luís Pereira<sup>1,2</sup> , José Xavier<sup>1,3,4</sup> , Bahman Ghiassi<sup>5</sup>,  
José Lousada<sup>1</sup> and José Morais<sup>1,4</sup>

## Abstract

This work addresses the reconstruction of strain gradient fields at the wood growth ring scale from full-field deformation measurements provided by digital image correlation. Moreover, the spatial distribution of the earlywood and latewood radial modulus of elasticity is assessed. Meso-scale tensile tests are carried out on *Pinus pinaster* Ait. wooden specimens oriented in the radial–tangential plane under quasi-static loading conditions. A parametric analysis of the two-dimensional digital image correlation extrinsic and intrinsic setting parameters is performed, in a balance between spatial resolution and resolution. It is shown that the parametric module is an effective way to quantitatively support the choice of digital image correlation parameters in the presence of the high deformation gradient fields generated by the structure–property relationships at the scale of observation. Under the assumption of a uniaxial tensile stress state, the spatial distribution of the radial elastic modulus across the growth rings is obtained. It is observed that the ratio of the radial modulus of elasticity between latewood and earlywood tissues can vary significantly as a function of the digital image correlation parameters. It is pointed out, however, that a convergence value can be systematically established. Effectively, earlywood and latewood stress–strain curves are obtained and elastic properties are determined assuming the converged digital image correlation setting parameters.

## Keywords

Wood, digital image correlation, earlywood, latewood, mechanical tensile test

Date received: 3 March 2018; accepted: 8 June 2018

## Introduction

In recent decades, wood and wood-based products have been increasingly used as engineering materials, gaining momentum from policies of sustainable development. Wood is a complex, hierarchical, anisotropic and heterogeneous material formed in the growing process of a tree. In softwood, tracheids are elongated cells forming an orthotropic structure, with three mutually orthogonal axes: the longitudinal (L) direction along tracheids and the radial (R) and tangential (T) directions in the transverse plane of tracheids. At the macroscopic scale (clear wood), two levels of heterogeneity can be distinguished within the stem. At the growth ring scale (1–10 mm), earlywood and latewood cellular tissues are observed, with distinct physical and mechanical properties.<sup>1–5</sup> At the stem scale (> 1 m), heterogeneities are revealed by radial and longitudinal variations on both physical and mechanical properties.<sup>6–9</sup> To assess wood

quality, the mechanical properties of wood species integrating these heterogeneities must be accurately characterised by suitable approaches.<sup>10,11</sup> Local properties at the meso growth ring scale can be of importance in

<sup>1</sup>Centre for the Research and Technology of Agro-Environmental and Biological Sciences (CITAB), University of Trás-os-Montes and Alto Douro (UTAD), Vila Real, Portugal

<sup>2</sup>DEMad and ESTG, Polytechnic Institute of Viseu, Viseu, Portugal

<sup>3</sup>Laboratory of Optics and Experimental Mechanics (LOME), Institute of Science and Innovation in Mechanical and Industrial Engineering (INEGI), Porto, Portugal

<sup>4</sup>Escola de Ciências e Tecnologia, University of Trás-os-Montes and Alto Douro (UTAD), Vila Real, Portugal

<sup>5</sup>Centre for Structural Engineering and Informatics, The University of Nottingham, Nottingham, UK

## Corresponding author:

José Xavier, Escola de Ciências e Tecnologia, University of Trás-os-Montes and Alto Douro (UTAD), Quinta de Prados, 5000-801 Vila Real, Portugal.  
Email: jmcx@utad.pt

applications dealing with fracture mechanics of wooden structures<sup>12</sup> and wood joints,<sup>13</sup> since the region of analysis of the observed phenomena is comparable to the size of the growth rings. Thus, in order to enhance wood application, not only the bulk mechanical properties but also their spatial variability must be accurately characterised by suitable methodologies. Currently, standard testing mechanical approaches are, however, limited by their restrictive assumptions (e.g. homogeneity, uniaxial stress states).

Experimental solid mechanics rely on surface deformation measurements. Simplified assumptions are commonly invoked in the test mechanical models based on a uniform/linear stress field at the gauge section. Hence, closed-form solutions for material parameters as a function of specimen dimensions, applied load and deformation are proposed in standard test methods. Therefore, punctual measurements can be carried out using strain gauges or extensometers. This macroscopic approach, however, is not suitable to properly tackle the problem of spatial variability of mechanical properties due to the structure–property relationships that can be observed, for instance, at the growth ring scale of the wood tissue. The recent progress on digital cameras and image processing and analysis has allowed the development of novel optical methods in the field of experimental solid mechanics.<sup>14–17</sup> These methods can be classed into white-light and interferometric techniques, considering the physical phenomenon emerging on the measurements. They provide full-field data and contact free, in contrast to piecewise measurement techniques. Among them, digital image correlation (DIC)<sup>18–22</sup> and grid methods<sup>8,23–26</sup> have been increasingly used due to its simplicity, relative good balance between spatial resolution and accuracy and coupling facilities to universal testing machines. In the following, the two-dimensional (2D)-DIC technique is highlighted due to its relevance to the presented research work. In particular, the subset-based correlation method is used. Up to date, commercial software have been subset-based oriented, although other approaches have been proposed such as the Fourier-based DIC<sup>27</sup> and the (global) finite element–based DIC.<sup>28–30</sup> Despite relevant achievements and increasingly utilisation of DIC, this technique is still not standardised. It is pointed out that DIC extrinsic and intrinsic setting parameters such as subset size, subset step, strain gauge window, shape functions or correlation criterion can have a tremendous influence on the computed deformation fields, yielding spatial resolution and resolution values that may differ of, at least, one order of magnitude.<sup>31–34</sup> Therefore, they are key issues when using DIC for displacement and strain measurements. Moreover, the experimental uncertainties can influence the identification of relevant mechanical material properties.<sup>35,36</sup> Due to the anisotropy and heterogeneity of wood, the application and relevance of optical methods in measuring wood deformation have been highlighted in several works.<sup>4,8,24,25,37–44</sup>

This work dealt with the reconstruction of the spatial variation of the modulus of elasticity in the radial direction ( $E_R$ ) between earlywood and latewood tissues of *Pinus pinaster* Ait. wood from full-field deformation measurements. Meso-scale tensile tests were carried out on radial-oriented specimens under quasi-static loading conditions (viscoelastic and inertia effects were neglected). Measurements were coupled with DIC to assess the deformation gradients across the central gauge area covering a few annual growth rings. A parametric study was performed analysing the influence of the selected DIC setting parameters on the reconstructed strain fields. Moreover, the effect of these choices on the spatial distribution and identification of earlywood and latewood radial elastic moduli was discussed.

## Methods

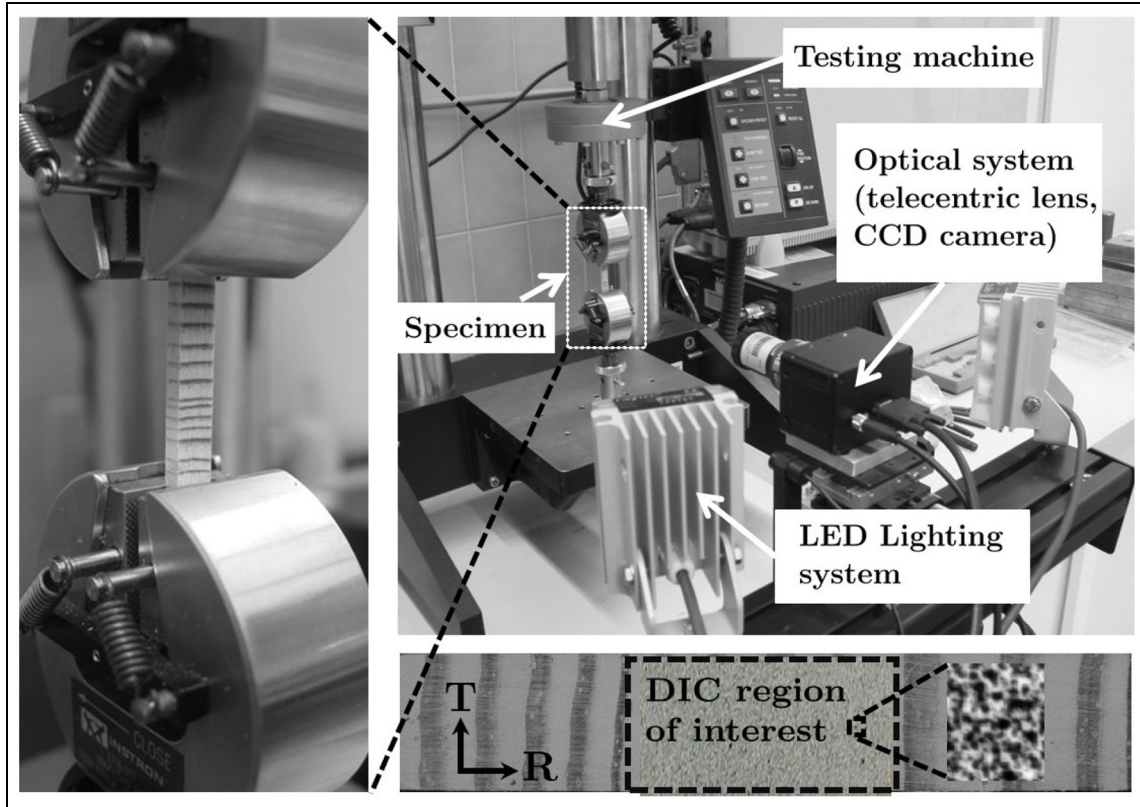
### Material and specimen

The wood specimens tested in this work were manufactured from a *P. pinaster* trees aged 70 years (origin: central-northern region of Portugal). From the basal log, 10 matched, clear wood specimens were cut on the radial–tangential (RT) plane with nominal dimensions of 50 (R) × 7 (T) × 2 (L) mm<sup>3</sup>. The growth ring structure of the specimen is shown in Figure 1, framed with the mechanical set-up. As it is noticed, at the measured scale, the central part of the specimen covers typically a few growth rings. The specimens were kept in the laboratory environmental conditions in order to reach their equilibrium moisture content before testing. According to ASTM D4442-16 Standard,<sup>45</sup> the specimen moisture content was determined around 10%–12%. Following the ASTM D2395-17 Standard,<sup>46</sup> specimen density was measured between 0.546 and 0.780 g cm<sup>-3</sup>. Moreover, the density profiles across the specimens were measured by means of X-ray microdensitometry.<sup>9</sup> From these measurements, an average density of  $\rho = 0.700$  g cm<sup>-3</sup> was obtained across the growth rings. Moreover, earlywood and latewood densities of 0.455 (–34.97%) g cm<sup>-3</sup> and 0.976 (+ 39.54%) g cm<sup>-3</sup> with a ratio of 2.1 were determined.

### Mechanical tensile test

The material parameters governing relevant constitutive models of a material are determined experimentally by means of suitable mechanical tests. In this work, a uniaxial tensile test was carried out on the RT growth ring specimens as shown in Figure 1. The mechanical test was coupled with DIC to assess full-field measurements across the central gauge area of 7.1 (R) × 5.4 (T) mm<sup>2</sup>.

The tensile mechanical tests were performed on an MicroTester machine (model 5848; Instron, Barcelona, Spain) under displacement control of 0.2 mm min<sup>-1</sup> (Figure 1). The load was measured by a 2 kN load cell. Tests were carried out under quasi-static conditions



**Figure 1.** Meso-tensile tests on radial–tangential wooden specimen with nominal dimensions of  $50 (R) \times 7 (T) \times 2 (L) \text{ mm}^3$ , with a full-field DIC region of interest of  $7.1 (R) \times 5.4 (T) \text{ mm}^2$ .

with a strain rate of  $\dot{\varepsilon} = 10^{-4} \text{ s}^{-1}$ . Load was applied monotonically throughout the test, in which both viscoelastic and inertia effects were therefore neglected.

## DIC

The 2D-DIC technique provides the measurement of the displacement field of a planar object by correlating textured (e.g. speckled) patterns between pair of images recorded before and after deformation.<sup>18</sup> The size of the subset patterns in the image defines the spatial resolution of the method. These data represent a field of displacement vectors across the region of interest. The imaged surface must have a random, contrasted, isotropic and uniform pattern to enhance the intensity-based matching algorithm. In contrast to the finite element method, adjacent subsets can overlap to improve the strain spatial resolution. Several mathematical correlation criteria have been proposed to determine the displacement components in the subset correlation process.<sup>19</sup> They measure the similarity of grey-level distributions around a given pixel between images recorded before and after deformation. A simple correlation criterion can be defined as follows<sup>19,47</sup>

$$C(x, y, x', y') = \frac{\sum_{\Omega} F(x, y)G(x', y')}{\sqrt{\sum_{\Omega} F(x, y)^2 \sum_{\Omega} G(x', y')^2}} \quad (1)$$

where  $\Omega$  is the subset domain,  $F(x, y)$  represents the value of the light intensity recorded at location  $(x, y)$  in the reference image, and  $G(x', y')$  represents the grey-level intensity at coordinate  $(x', y')$  in the deformed image. Nevertheless, other correlation criteria have been used such as the zero-normalised sum of squared differences (ZNSSD). The latter is a least-square-based correlation criterion which is less sensitive to both image contrast reduction and light intensity shifting between images. However, the ZNSSD algorithm has a more complex numerical implementation. This correlation criterion is particularly recommended in stereo-correlation (stereo-DIC or DIC 3D (three-dimensional)) measurements because of light intensity variance between the two recorded cameras. Equation (1) is solved with regard to the deformation parameter that defines the mapping function. Depending on the local deformation or strain gradients of the problem under analysis, affine, irregular and quadratic shape functions can be selected by the user in the DIC method. In particular, first-order or second-order shape functions can be written in Taylor series expansion, respectively, as follows

$$\begin{cases} x' = x_0 + \Delta x + u_x + \frac{\partial u_x}{\partial x} \Delta x + \frac{\partial u_x}{\partial y} \Delta y \\ y' = y_0 + \Delta y + u_y + \frac{\partial u_y}{\partial x} \Delta x + \frac{\partial u_y}{\partial y} \Delta y \end{cases} \quad (2)$$

and

$$\begin{cases} x' = x_0 + \Delta x + u_x + \frac{\partial u_x}{\partial x} \Delta x + \frac{\partial u_x}{\partial y} \Delta y + \\ \quad + \frac{1}{2} \frac{\partial^2 u_x}{\partial x^2} \Delta x^2 + \frac{1}{2} \frac{\partial^2 u_x}{\partial y^2} \Delta y^2 + \frac{\partial^2 u_x}{\partial x \partial y} \Delta x \Delta y \\ y' = y_0 + \Delta y + u_y + \frac{\partial u_y}{\partial x} \Delta x + \frac{\partial u_y}{\partial y} \Delta y + \\ \quad + \frac{1}{2} \frac{\partial^2 u_y}{\partial x^2} \Delta x^2 + \frac{1}{2} \frac{\partial^2 u_y}{\partial y^2} \Delta y^2 + \frac{\partial^2 u_y}{\partial x \partial y} \Delta x \Delta y \end{cases} \quad (3)$$

An optimisation problem is then formulated by minimising the correlation criterion (equation (1)) with regard to the deformation parameters (equation (2) or (3)). The solution of this problem is often sought by means of a Newton–Raphson or Levenberg–Marquardt iteration algorithm in finding the optimal set of deformation parameters for the correlation coefficient.<sup>19,47,48</sup>

The DIC setting parameters must be selected in post-processing the recorded images. They represent fundamental parameters since they will contribute to the spatial resolution ( $\Delta u$ ) and resolution ( $\sigma_u$ ) associated with the DIC measurements. Therefore, they must be carefully chosen with regard to the end-user application, in a compromise between correlation (small subsets) and interpolation (large subsets) errors. The first (external) global parameter is the subset size ( $f_s$ ). It defines the correlation window over which the matching algorithm operates between pairs of images, recorded before and after deformation. The lower pixel boundary is constrained by aliasing effects, which is typically defined by the size of the speckle (or texture) on the imaged pattern. A rule of thumb will be three isotropic and contrasted speckles or features per subset. The upper pixel limit can be problem-dependent taking into account the deformation gradients expected within the region of interest, in a balance between spatial resolution and resolution. As a guideline, larger subsets improve the resolution but decreases spatial resolution. This means that on a classical mechanical tensile test, with uniform and uniaxial state of stress at the central region of the specimen (*Saint-Venant's* principle), large subsets may be selected enhancing the accuracy of the measurements. In this study, however, due to the material meso (annual growth ring) structure, heterogeneous strains fields are expected, generated by the different elastic properties of earlywood and latewood tissues. Parameters such as the subset step ( $f_p$ ) (distance between centroids of adjacent subsets, unit: pixels) and the strain window  $\varepsilon_w$  (number of subsets central points used to define a mesh of data points over which a piecewise polynomial fitting will be applied, using least-square regression, for strain reconstruction) will define a strain spatial resolution ( $\Delta \varepsilon$ ) and virtual strain gauge (VSG), respectively, according to the following relationships:<sup>49</sup>  $\Delta \varepsilon = (\varepsilon_w - 1)f_p + f_s$  and  $VSG = (\varepsilon_w - 1)f_p + 1$  (unit: pixels). For convenience, these parameters can be converted to physical units in the object space (e.g. mm), by simple multiplication by the conversion factor of the optical imaging system. All these external DIC parameters, therefore, must be carefully selected in this study.

**Table 1.** DIC setting parameters used in the parametric analysis of the MatchID software.

Correlation setting – subset	
Size	{11, 21, 31, 41, 51, 61}
Step	{9, 14, 19, 24, 29}
Shape function	{Affine, Quadratic}
Strain derivation settings	
Strain window	{3, 7, 11, 15}
Polynomial order <sup>a</sup>	{Bilinear (Q4), Biquadratic (Q8)}

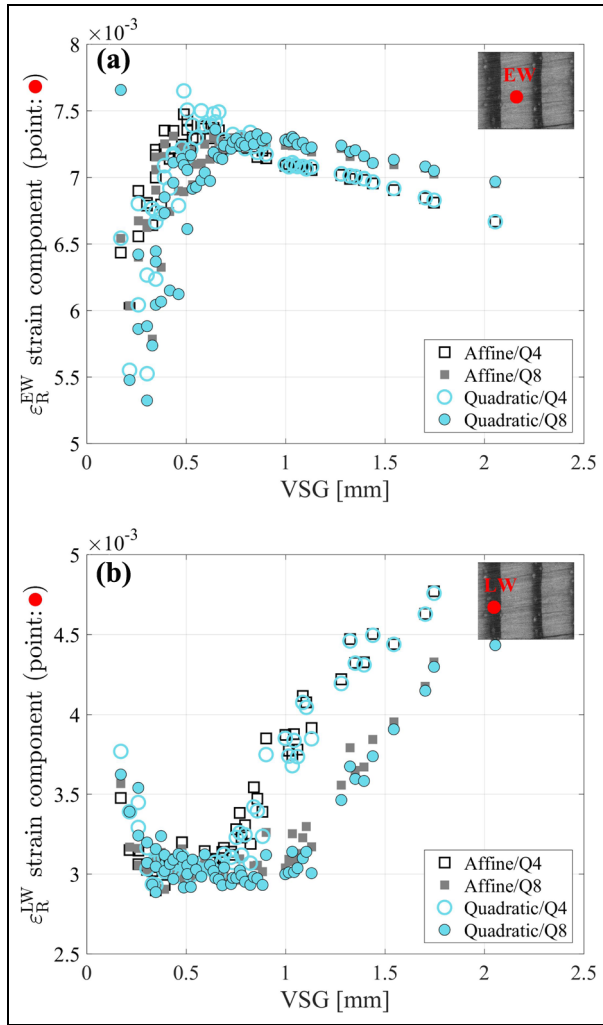
<sup>a</sup>Point-wise local least-squares fitting approach for the reconstruction of the strain fields from the displacement data points.

In this work, an optical system equipped with a Baumer Optronic FWX20 camera (8 bits,  $1624 \times 1236$  pixels<sup>2</sup>) was used coupled with a telecentric lens (model TC 23 09; Opto Engineering SRL, Mantova, Italy), as shown in Figure 1. The working distance was defined to 103.5 mm, yielding a pixel conversion factor of  $4.4 \mu\text{m pixel}^{-1}$ . Images were recorded at an acquisition frequency of 1.0 Hz. Two LED lighting sources (Raylux 25 white-light; Raytec Ltd, Ashington, UK) were used to guarantee uniform illumination and to avoid significant heating of the specimens.

## Results

### DIC: parametric analysis

The DIC setting parameters must be selected in post-processing the speckled pattern images recorded during the mechanical tensile tests. In the current application, however, due to the meso-scale magnification, a careful choice must be made for the true signal reconstruction, in the best compromise between spatial resolution and accuracy. To accomplish this purpose, a parametric analysis was carried out using the MatchID DIC software.<sup>50</sup> Considering the high-strain gradient fields generated by the wood growth ring structure, the parametric module allowed to approach the DIC analysis in a quantitative way. A parametric study was carried out considering the setting parameters reported in Table 1. For each type of parameter, a practical range was assumed. The set of different combinations (in a total of 240 analyses) corresponds to a VSG range in between 39 and 467 pixels. The Green–Lagrange tensor was used for strain computation. For the sake of simplicity, in this study, a single pair of data points in the earlywood and latewood tissues was considered. Figure 2 summarises the results from this analysis. To start with, the radial strain ( $\varepsilon_R^{EW}$ ) reconstruction on earlywood (EW) tissue with regard to VSG is presented in the  $\varepsilon_R^{EW}$  – VSG data curve as a parametric function of the DIC input settings (Figure 2(a)). As it can be concluded, the convergence to a value of about  $\varepsilon_R^{EW} \simeq 7.25 \times 10^{-3}$  is reached around a VSG in between 0.5 and 1.0 mm. If DIC parameters are selected in a



**Figure 2.** DIC parametric analysis: (a)  $\varepsilon_R^{EW}$  strain component and (b)  $\varepsilon_R^{LW}$  strain component (applied load of 110 N).

way that larger VSGs are obtained, the strain signal reconstruction decreases because of the influence of latewood tissue deformation. Small VSG seems also to underestimate the strain values at the earlywood layer. By analogy, the strain reconstruction on latewood (LW) tissue with regard to VSG is presented in the  $\varepsilon_R^{LW}$  – VSG data curve (Figure 2(b)). In this case study, a convergence was reached at about  $\varepsilon_R^{LW} \simeq 3 \times 10^{-3}$  in the VSG range of 0.5–1.0 mm. The value of radial strain in latewood increases for larger VSG because of the influence of earlywood tissue, which deforms more at a given stress state. Furthermore, from the analysis on both tissues, it can be concluded that affine (first-order) or quadratic (second-order) shape functions yield equivalent results. Moreover, bilinear or biquadratic piecewise polynomials, used in the reconstruction of the strain fields from the displacement data points, seem to reach the same type of convergence.

The DIC parametric analysis was extended to assess the  $E_R$  ratio between earlywood and latewood tissues. Assuming equilibrium and constitutive linear elastic behaviour under the uniaxial tensile test, the following proportional relationship is obtained:  $E_R^{LW}/E_R^{EW} \propto$

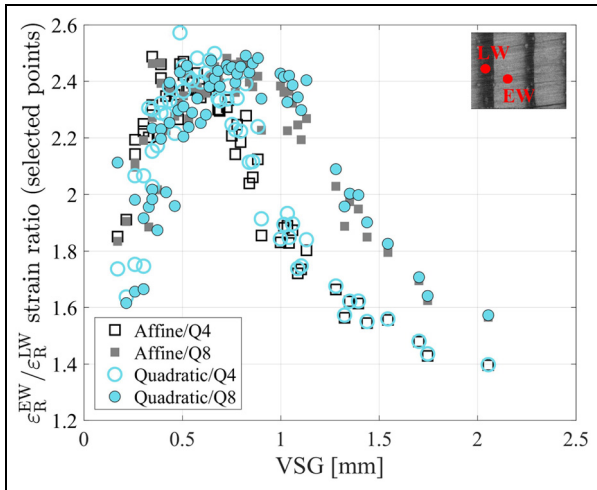
$\varepsilon_R^{EW}/\varepsilon_R^{LW}$ . Figure 3 shows the evaluation of  $\varepsilon_R^{EW}/\varepsilon_R^{LW}$  with regard to the VSG for the DIC parametric analysis. As it can be observed, a huge scatter on the data (ratios in between 1.4 and 2.6) is obtained as a function of the DIC setting parameters. These results clearly point out the necessity of a well-balanced reconstruction of the strain gradient fields when dealing with this level of material heterogeneity. Nevertheless, over the analysed range of VSG, a convergence ratio can be systematically estimated from the data of Figure 3. Although this analysis was presented over a single pair of representative points in the earlywood and latewood tissues, similar conclusions could be obtained across the region of interest, and the anisotropic ratio quantitatively evaluated on a statistical basis.

### Strain fields and radial elastic modulus distribution

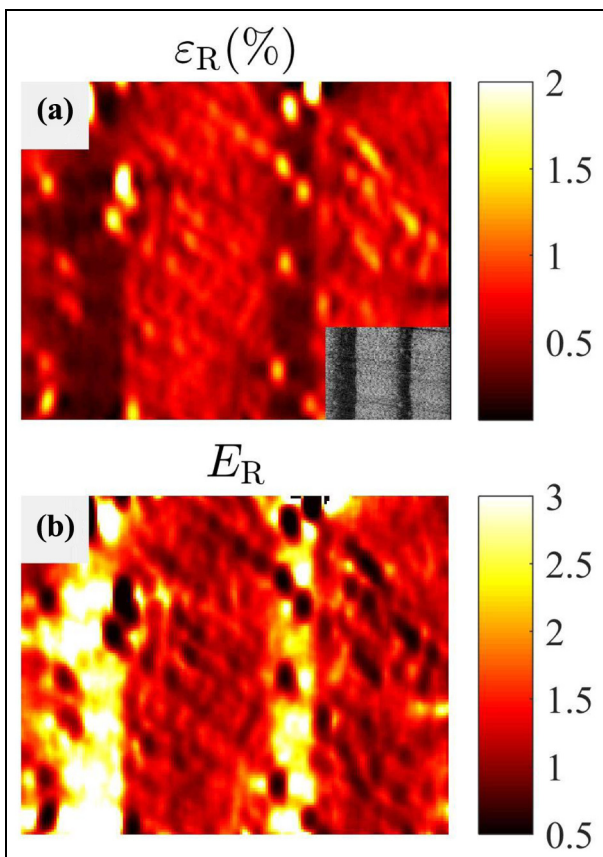
A qualitative evaluation of the radial strain field ( $\varepsilon_R$ ) across the growth ring gauge section is presented in Figure 4(a), for a given sample. This field was obtained for the following DIC setting parameters: subset size – 21, subset step – 9, strain window – 7, correlation criterion – zero-normalised sum of squared differences (ZNCC), image interpolation – bicubic spline interpolation, image prefiltering – Gaussian  $5 \times 5$  kernel, shape function – quadratic, piecewise strain reconstruction – bilinear quadrilateral (Q4). From the  $\varepsilon_R$  strain field and assuming linear elastic behaviour under uniaxial stress state, the map of the radial modulus of elasticity across the gauge section was reconstructed as shown in Figure 4(b). As can be seen, both radial strain and elastic modulus were consistent with the material meso-structure at the scale of observation. The latter field provided a full-field overview of the estimated spatial variation of the  $E_R$  elastic modulus within the growth ring structure. The mean radial modulus of elasticity along each section follows, as expected, the variation of the local density profile (see Figure 4(a)), in which earlywood tissue has a lower modulus with regard to the latewood counterpart layer.

### Global and local stress–strain relationships

A growth ring image classification was performed by mapping earlywood and latewood areas across the DIC region of interest. To start with, a simple threshold method was first applied to the original textured tissue pattern (as seen in Figure 1) to obtain a binary image with the segmented earlywood and latewood layers. This operation, however, was typically performed with uncertainty, namely, in the earlywood to latewood transition because of a bright-to-bark unclear definition. To cope with this issue, morphological operations were implemented based on a sequence of erosion and dilation operations. The disc morphological structure element with a kernel of  $3 \times 3$  pixels was used. This analysis is exemplified in Figure 5 where earlywood and latewood segmented masks are plotted together with

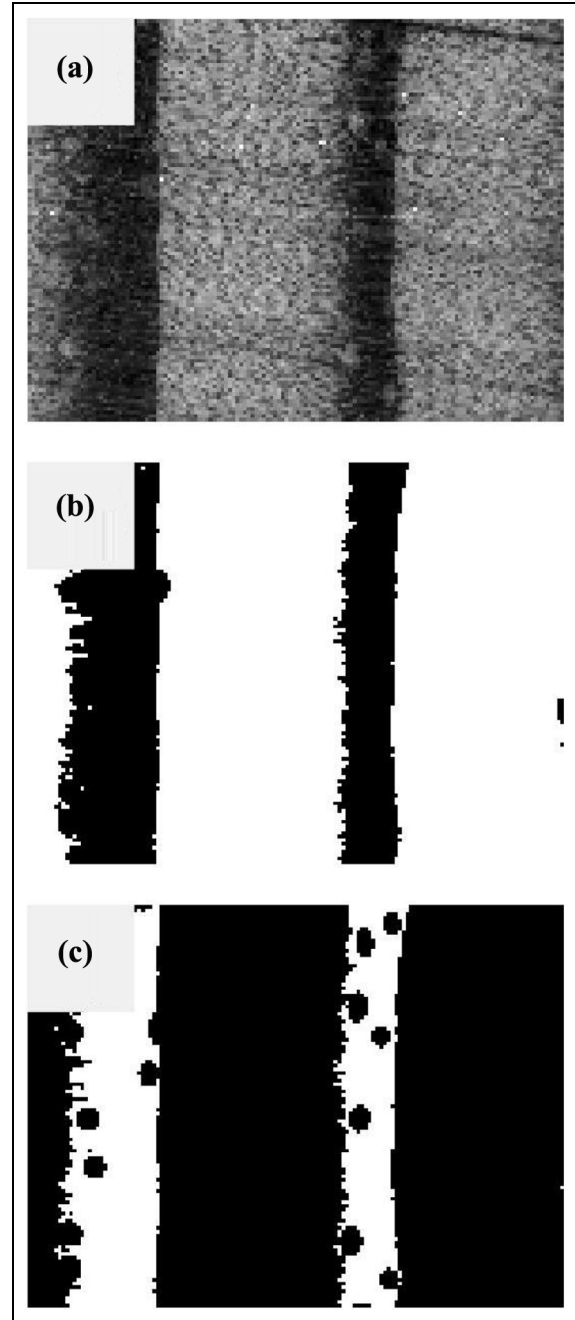


**Figure 3.** Reconstruction of the earlywood to latewood ratio of the radial strain components ( $\epsilon_R^{EW}/\epsilon_R^{LW}$ ) as a function of the DIC setting parameters used in the parametric analysis (Table 1). (Under the assumption of uniaxial stress state, the data points can also be understood as the ratio of the radial modulus of elasticity between latewood and earlywood tissues,  $E_R^{LW}/E_R^{EW}$ ).



**Figure 4.** (a) Radial strain field ( $\epsilon_R$ ) and (b) radial modulus of elasticity map across the meso-scale gauge area ( $E_R$ ) (calculated from  $\epsilon_R$  assuming linear elastic behaviour under uniaxial stress state).

the original growth ring structure. These masks will then be used to segment the strain field components and therefore to decompose the global stress–strain



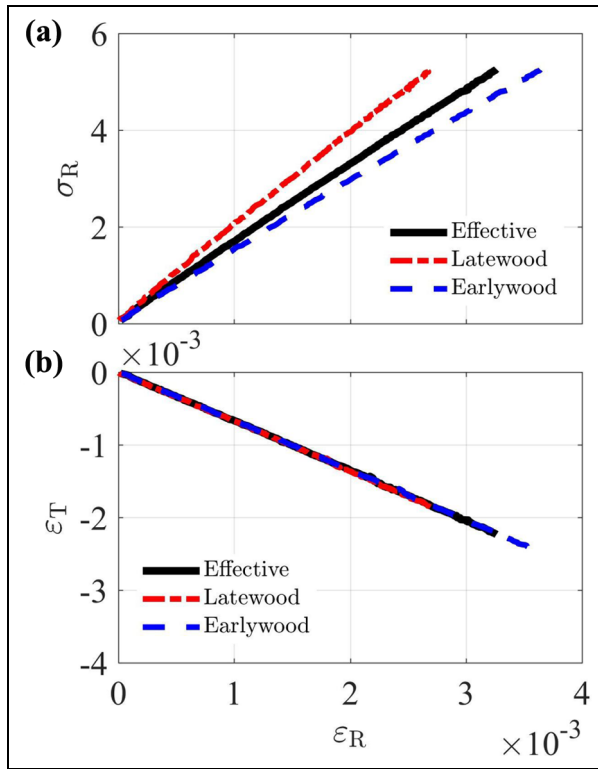
**Figure 5.** (a) Growth ring structure, (b) latewood segmented mask and (c) earlywood segmented mask.

curve into local earlywood and latewood mechanical responses.

From load and images recorded simultaneously during the tensile test, global stress–strain curves were determined. The uniaxial nominal tensile stress ( $\sigma_R$ ) was simply defined as load divided by initial cross section of the specimens. The linear strain components ( $\epsilon_R$  and  $\epsilon_T$ ) were then measured as the average of the strain field components across the overall region of interest. These mean values were understood as macro-measurements of the strain components since they do integrate a few annual growth rings at the gauge section.

**Table 2.** Effective, earlywood and latewood radial modulus of elasticity ( $E_R$ ) and Poisson's ratio ( $\nu_{RT}$ ).

	$E_R$ (MPa)	$E_R^{EW}$ (MPa)	$E_R^{LW}$ (MPa)	$\nu_{RT}$	$\nu_{RT}^{EW}$	$\nu_{RT}^{LW}$
Mean	1.698	1.578	1.945	0.607	0.631	0.604
Standard deviation	0.07	0.106	0.111	0.051	0.053	0.044
Coefficient of variation (%)	4.14	6.72	5.70	8.38	8.46	7.30

**Figure 6.** Effective, earlywood and latewood elastic typical mechanical response: (a)  $\sigma_R - \epsilon_R$  curves and (b)  $\epsilon_T - \epsilon_R$  curves.

Considering the segmented masks provided by the image processing and analysis (Figure 5), effective, earlywood and latewood  $\sigma_R - \epsilon_R$  and  $\epsilon_T - \epsilon_R$  curves were reconstructed in the linear elastic domain as shown in Figure 6(a) and (b), respectively. In a qualitative evaluation of  $E_R$ , a higher value is expected to be associated with latewood in regard to earlywood. Besides, a small variation of  $\nu_{RT}$  is expected due to the close slope of the  $\epsilon_T - \epsilon_R$  curves (Figure 5(b)). Qualitatively, from these curves, the effective, earlywood and latewood radial modulus of elasticity ( $E_R$ ) and Poisson's ratio ( $\nu_{RT}$ ) were determined by least-square regression. Table 2 summarises the obtained values. These values are consistent with reference ones reported in the literature.<sup>7,9</sup>

## Discussion

The deformation of wood can be quite complex due to its anisotropy and heterogeneity. Full-field deformation measurements were carried out at the growth ring scale using DIC. This technique was confirmed to be effective for this type of measurements at the observed scale of

magnification. However, due to the high-strain gradient fields engendered by the growth ring structure, the selection of the DIC setting parameters was not a trivial task in this application. It was pointed out that the reconstructed radial strain component and therefore the estimated  $E_R$  ratio between latewood and earlywood were very dependent on the DIC setting parameters. Nevertheless, it was shown that the parametric analysis was a quantitative way to address this issue. A convergence path was observed proving the consistency of measurements and therefore the identification of spatial distribution of properties in between tissues. The latewood/earlywood  $E_R$  ratio was of the same order of the latewood/earlywood density ratio, suggesting an approximated linear relationship between density and elastic radial modulus. This is in agreement with independent studies.<sup>7,51</sup>

## Conclusion

Meso-scale tensile tests coupled with full-field measurements provided by DIC were successfully carried out on RT *P. pinaster* specimens to assess the local deformation of earlywood and latewood constituents. A DIC parametric analysis was performed to quantitatively analyse the reconstruction of the strain fields across the heterogeneous growth ring structure, on a compromise between spatial resolution and resolution. It was observed that the ratio of the radial modulus of elasticity between latewood and earlywood tissues can vary significantly as a function of the DIC parameters. It was pointed out, however, that a convergence value can be statistically established. Effectively, earlywood and latewood stress-strain curves and elastic parameters were determined assuming a uniaxial tensile stress state from the converged DIC setting parameters. These data are in agreement with reference values in the literature.

## Declaration of conflicting interests


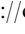
The author(s) declared no potential conflicts of interest with respect to the research, authorship, and/or publication of this article.

## Funding

The author(s) disclosed receipt of the following financial support for the research, authorship, and/or publication of this article: This work is supported by

European Investment Funds by FEDER/COMPETE/POCI – Operacional Competitiveness and Internationalization Programme, under Project POCI-01-0145-FEDER-006958 and National Funds by FCT – Portuguese Foundation for Science and Technology, under the project UID/AGR/04033/2013.

### ORCID iDs

João Luís Pereira  <https://orcid.org/0000-0002-9916-558X>  
 José Xavier  <https://orcid.org/0000-0002-7836-4598>

### References

- Watanabe U, Fujita M and Norimoto M. Transverse Young's moduli and cell shapes in coniferous early wood. *Holzforschung* 2002; 56(1): 1–6.
- Thuvander F, Jernkvist L and Gunnars J. Influence of repetitive stiffness variation on crack growth behaviour in wood. *J Mater Sci* 2000; 35(24): 6259–6266.
- Farruggia F and Perré P. Microscopic tensile tests in the transverse plane of earlywood and latewood parts of spruce. *Wood Sci Technol* 2000; 34(2): 65–82.
- Dang D, Pitti RM, Toussaint E, et al. Inverse identification of early- and latewood hydric properties using full-field measurements. *Wood Mater Sci Eng* 2018; 13(1): 50–63.
- Cramer S, Kretschmann D, Lakes R, et al. Earlywood and latewood elastic properties in loblolly pine. *Holz-forschung* 2005; 59(5): 531–538.
- Machado J and Cruz H. Within stem variation of maritime pine timber mechanical properties. *Holz Roh Werkst* 2005; 63(2): 154–159.
- Nairn J. A numerical study of the transverse modulus of wood as a function of grain orientation and properties. *Holzforschung* 2007; 61(4): 406–413.
- Xavier J, Avril S, Pierron F, et al. Variation of transverse and shear stiffness properties of wood in a tree. *Compos Part A: Appl S* 2009; 40(12): 1953–1960.
- Pereira JLE, Xavier J, Morais J, et al. Assessing wood quality by spatial variation of elastic properties within the stem: case study of *Pinus pinaster* in the transverse plane. *Can J Forest Res* 2014; 44(2): 107–117.
- Tsehaye A, Buchanan A and Walker J. Selecting trees for structural timber. *Holz Roh Werkst* 2000; 58(3): 162–167.
- Wagner L, Bader T, Auty D, et al. Key parameters controlling stiffness variability within trees: a multiscale experimental–numerical approach. *Trees: Struct Funct* 2013; 27(1): 321–336.
- Holmberg S, Persson K and Petersson H. Nonlinear mechanical behaviour and analysis of wood and fibre materials. *Comput Struct* 1999; 72(4–5): 459–480.
- Santos C, de Jesus A, Morais J, et al. Quasi-static mechanical behaviour of a double-shear single dowel wood connection. *Constr Build Mater* 2009; 23(1): 171–182.
- Rastogi P (ed.). *Photomechanics*. Berlin: Springer-Verlag, 2000.
- Sciammarella C and Sciammarella F. *Experimental mechanics of solids*. New York: John Wiley & Sons, 2012.
- Rastogi PK and Hack E (eds). *Optical methods for solid mechanics: a full-field approach*. New York: John Wiley & Sons, 2012.
- Grédiac M and Hild F (eds). *Full-field measurements and identification in solid mechanics*. New York: John Wiley & Sons, 2012.
- Sutton M, Orteu JJ and Schreier H. *Image correlation for shape, motion and deformation measurements: basic concepts, theory and applications*. New York: Springer, 2009.
- Pan B, Qian K, Xie H, et al. Two-dimensional digital image correlation for in-plane displacement and strain measurement: a review. *Meas Sci Technol* 2009; 20(6): 062001.
- Xavier J, Oliveira M, Monteiro P, et al. Direct evaluation of cohesive law in mode I of *Pinus pinaster* by digital image correlation. *Exp Mech* 2014; 54(5): 829–840.
- Catalanotti G and Xavier J. Measurement of the mode II intralaminar fracture toughness and R-curve of polymer composites using a modified Iosipescu specimen and the size effect law. *Eng Fract Mech* 2015; 138: 202–214.
- Kuhn P, Catalanotti G, Xavier J, et al. Fracture toughness and crack resistance curves for fiber compressive failure mode in polymer composites under high rate loading. *Compos Struct* 2017; 182: 164–175.
- Grédiac M, Blaysat B and Sur F. A critical comparison of some metrological parameters characterizing local digital image correlation and grid method. *Exp Mech* 2017; 57(6): 871–903.
- Xavier J, Avril S, Pierron F, et al. Novel experimental approach for longitudinal-radial stiffness characterisation of clear wood by a single test. *Holzforschung* 2007; 61(5): 573–581.
- Xavier J, Belini U, Pierron F, et al. Characterisation of the bending stiffness components of MDF panels from full-field slope measurements. *Wood Sci Technol* 2013; 47(2): 423–441.
- Rossi M and Pierron F. On the use of simulated experiments in designing tests for material characterization from full-field measurements. *Int J Solids Struct* 2012; 49(3–4): 420–435.
- Su Y, Zhang Q, Gao Z, et al. Fourier-based interpolation bias prediction in digital image correlation. *Opt Express* 2015; 23(15): 19242–19260.
- Wang B and Pan B. Subset-based local vs. finite element based global digital image correlation: a comparison study. *Theor Appl Lett* 2016; 6(5): 200–208.
- Hild F and Roux S. Comparison of local and global approaches to digital image correlation. *Exp Mech* 2012; 52(9): 1503–1519.
- Réthoré J, Hild F and Roux S. Extended digital image correlation with crack shape optimization. *Int J Numer Meth Eng* 2008; 73(2): 248–272.
- Triconnet K, Derrien K, Hild F, et al. Parameter choice for optimized digital image correlation. *Opt Laser Eng* 2009; 47(6): 728–737.
- Kibitkin V, Solodushkin A, Pleshanov V, et al. On a choice of input parameters for calculation the vector field and deformation with DIC. *Measurement* 2017; 95: 266–272.
- Pan B, Xie H, Wang Z, et al. Study on subset size selection in digital image correlation for speckle patterns. *Opt Express* 2008; 16(10): 7037–7048.
- Yaofeng S and Pang J. Study of optimal subset size in digital image correlation of speckle pattern images. *Opt Laser Eng* 2007; 45(9): 967–974.



35. Rossi M, Lava P, Pierron F, et al. Effect of DIC spatial resolution, noise and interpolation error on identification results with the VFM. *Strain* 2015; 51(3): 206–222.
36. Badaloni M, Rossi M, Chiappini G, et al. Impact of experimental uncertainties on the identification of mechanical material properties using DIC. *Exp Mech* 2015; 55: 1411–1426.
37. Jernkvist L and Thuvander F. Experimental determination of stiffness variation across growth rings in *Picea abies*. *Holzforschung* 2001; 55(3): 309–317.
38. Hussain F, Nairn J and Muszynski L. An experimental method for measurement of strain distribution between wood the flour particles and polymer matrix on micro-mechanical level. *Mat Sci Eng A: Struct* 2011; 528(18): 6072–6078.
39. Majano-Majano A, Fernandez-Cabo J, Hoheisel S, et al. A test method for characterizing clear wood using a single specimen. *Exp Mech* 2012; 52(8): 1079–1096.
40. Xavier J, de Jesus A, Morais J, et al. Stereovision measurements on evaluating the modulus of elasticity of wood by compression tests parallel to the grain. *Constr Build Mater* 2012; 26(1): 207–215.
41. Xavier J, Fernandes JRA, Frazão O, et al. Measuring mode I cohesive law of wood bonded joints based on digital image correlation and fibre Bragg grating sensors. *Compos Struct* 2015; 121: 83–89.
42. Xavier J, Majano-Majano A and Fernandez-Cabo J. On the identifiability of stiffness components of clear wood from a 3D off-axes prismatic specimen: angle orientation and friction effects. *Eur J Wood Wood Prod* 2016; 74(3): 285–290.
43. Crespo J, Aira J, Vázquez C, et al. Comparative analysis of the elastic constants measured via conventional, ultrasound, and 3-D digital image correlation methods in *Eucalyptus globulus* Labill. *BioResources* 2017; 12(2): 3728–3743.
44. Toussaint E, Fournely E, Pitti RM, et al. Studying the mechanical behavior of notched wood beams using full-field measurements. *Eng Struct* 2016; 113: 277–286.
45. ASTM D4442–16. *Standard test methods for direct moisture content measurement of wood and wood-base materials*. ASTM International, West Conshohocken, PA, 2016.
46. ASTM D2395–17. *Standard test methods for density and specific gravity (relative density) of wood and wood-based materials*. ASTM International, West Conshohocken, PA, 2017.
47. Yoneyama S. Basic principle of digital image correlation for in-plane displacement and strain measurement. *Adv Compos Mater* 2016; 25(2): 105–123.
48. Bing P, Hui-min X, Bo-qin X, et al. Performance of sub-pixel registration algorithms in digital image correlation. *Meas Sci Technol* 2006; 17(6): 1615–1621.
49. Lava P, Paepegem WV, Coppieters S, et al. Impact of lens distortions on strain measurements obtained with 2D digital image correlation. *Opt Laser Eng* 2013; 51(5): 576–584.
50. MatchID. *MatchID Manual*. MatchID: Metrology beyond Colors, 2017.
51. Modén C and Berglund L. Elastic deformation mechanisms of softwoods in radial tension cell wall bending or stretching? *Holzforschung* 2008; 65(14): 562–568.